

ML Time-Delay and CFO Synchronization for MIMO-Relay Beamforming over Time-Varying Channels

Souheib Ben Amor*, Sofiène Affes*, Faouzi Bellili[†], Usa Vilaipornasawai[†], Liqing Zhang[†], and Peiying Zhu[†]

*INRS-EMT, Université du Québec, Montréal, QC, Canada, Emails: {souheib.ben.amor, affes}@emt.inrs.ca

[†] University of Toronto, Toronto, ON, Canada, Emails: faouzi.bellili@utoronto.ca

[†]Huawei Technologies Canada Co. Ltd., Kanata, ON, Canada, Emails: {usa.vilaipornasawai, liqing.zhang, peiying.zhu}@huawei.com

Abstract—In this paper, we investigate maximum likelihood (ML) time delay (TD) and carrier frequency offset (CFO) synchronization (i.e., estimation and pre-compensation) in decode-and-forward (DF) cooperative systems operating over time-varying channels (TVCs). The new technique is embedded at each relay node in order to avoid the drawbacks of multidimensional ML estimation at the destination and to minimize the overhead cost. By accounting for a perfect Doppler spread value, the new synchronization solution delivers accurate TD and CFO estimates at each relay. The resulting TD and CFO estimates along with the channel estimates are then exploited by the MIMO relay for precompensation at each node of the distributed transmit beamforming signals to ensure constructive maximum ratio combining (MRC) at the destination. Simulation results show significant synchronization accuracy improvement over previous distributed multi-node synchronization techniques assuming time-constant channels (TCCs). The latter translates into noticeable gains in terms of useful (i.e., after accounting for incurred overhead) link-level throughput, more so at higher Doppler.

Index Terms—Carrier Frequency Offset (CFO), Time Delay (TD), Time-Varying Channel (TVC), Doppler Spread, Distributed MIMO Relay Beamforming, Cooperation, Decode-and-Forward (DF), Multi-Node Synchronization, Maximum Likelihood (ML).

I. INTRODUCTION

Spatial diversity is a well-known concept allowing to combat the channel fading and increase the overall throughput of communication systems. Such attracting advantage can be achieved through multiple solutions. Cooperative networks provide a distributed solution that avoids some of the difficulties related to traditional MIMO systems [1, 2]. Indeed, in many situations, some user equipments are not able to embed multiple antenna sensors due to size and power limitations. As such, users can cooperate with each other to form a virtual antenna array. However, some challenges need to be addressed to ensure constructive cooperation between the relays. One major problem in cooperative relaying systems is multi-node

synchronization, both in time and frequency. The latter is crucial for the proper implementation of energy-, spectrum-, and area-efficient distributed MIMO-relay beamforming between a given source-destination link having coverage limitations.

There are two basic approaches to alleviate the effect of TVC distortions in time, frequency, phase, and amplitude: the closed-loop and the open-loop compensation procedures. In the closed-loop approach, the destination performs the estimation of all the synchronization parameters along with the channel coefficients. Those estimates are later fed to an equalization block to combat time and frequency asynchronism as proposed in [3,4]. To their credentials, closed-loop approaches exhibit less overhead as the interaction among the relay nodes is kept to minimal while the destination coordinates the synchronization process. However, it may be difficult for wireless networks without the adequate infrastructure to handle highly-complex multi-dimensional estimation algorithms. In open-loop approaches, however, the source signal to be relayed is shifted in the temporal and frequency domains before transmission, as proposed in [5]. By doing so, we ensure that replicas of the same transmitted signal, originating from different relay nodes, arrive at the same time and combine constructively at the receiver. In this scenario, less complex estimation algorithms can be considered at the nodes with minimal signaling from the destination.

As far as the estimation of the synchronization parameters is concerned, multiple techniques exist in the open literature. On one hand, the works in [6-9] investigate TD synchronization while neglecting the CFO's effect. On the other hand, the solutions introduced in [10-13] deal with multiple CFOs while neglecting the TD effect. It is also common to perform joint estimation of all parameters at the destination in closed-loop cooperative networks [3,14,15]. Although these solutions work very well in practice, they suffer from high computational complexity since they require solving a multi-dimensional problem that increases with the number of relaying nodes. Moreover, the synchronization task may become costly in terms of overhead. Indeed, after estimating the TDs and CFOs, the destination node needs to feed them back to the relays. Such step leads to an additional

Work supported by the NSERC/Huawei Canada/TELUS CRD Grant on 5G-WAVES (Wireless Access Virtualization Enabling Schemes), the DG and CREATE PERSWADE <www.create-perswade.ca> Programs of NSERC, and a Discovery Accelerator Supplement Award from NSERC.

overhead problem along with quantization errors since the estimated values are quantized before the feedback phase. An alternative solution can be considered by relying on distributed TD and CFO synchronization where the estimation process can be performed at each relay node instead of the receiver. In [16], a distributed synchronization method was proposed for dense wireless network using a correlation-based TD and CFO estimator. Yet, all the above-mentioned techniques rely on the simplifying TCC assumption. In contrast, fifth-generation (5G) communication systems are expected to support reliable communications at very high velocities reaching 500 Km/h (e.g., in high-speed trains) [17]. For such systems, the conventional TCC assumption leads to severe performance losses.

Motivated by these facts, we develop in this paper a new decentralized ML synchronization technique that tackles the challenging TVC case over multi-node relaying transmissions. The proposed ML TVC solution builds upon a very useful approximation of the channel covariance matrix by a two-ray propagation model. It provides accurate ML estimates of the TDs and CFOs at a reduced computational cost because it does not require any matrix inversion. Simulation results show significant synchronization accuracy improvement over previous distributed multi-node synchronization techniques assuming TCCs. The latter translates into noticeable gains in terms of useful (i.e., after accounting for incurred overhead) link-level throughput, more so at higher Doppler.

The rest of the paper is organized as follows. In Section II, we introduce the system model. In Section III, we derive the new ML solution of the underlying estimation problem. The pre-compensation procedure is presented in Section IV. In Section V, we run exhaustive computer simulations to assess the performance of the proposed distributed synchronization solution both at the component and link levels in terms of estimation accuracy and throughput, respectively. Finally, we draw out some concluding remarks in Section VI.

The notations adopted in this paper are as follows. Vectors and matrices are represented in lower- and upper-case bold fonts, respectively. Moreover, $\{\cdot\}^T$ and $\{\cdot\}^H$ denote the conjugate and Hermitian (i.e., transpose conjugate) operators and $\det\{\cdot\}$ returns the determinant of any square matrix. The Euclidean norm of any vector is denoted as $\|\cdot\|$ and \mathbf{I}_N denotes the $(N \times N)$ identity matrix. For any vector \mathbf{x} , $\text{diag}\{\mathbf{x}\}$ refers to the diagonal matrix whose elements are those of \mathbf{x} . For any matrix \mathbf{X} , $[\mathbf{X}]_q$ and $[\mathbf{X}]_{l,k}$ denote its q^{th} column and $(l, k)^{\text{th}}$ entry, respectively. The element-wise product between any two vectors \mathbf{x}_1 and \mathbf{x}_2 is denoted as $\mathbf{x}_1 \odot \mathbf{x}_2$. Moreover, $\{\cdot\}^*$, $\angle\{\cdot\}$, and $|\cdot|$ return the conjugate, angle, and modulus of any complex number, respectively. Finally, $\mathbb{E}\{\cdot\}$ stands for the statistical expectation, j is the imaginary unit (i.e., $j^2 = -1$), and the notation \triangleq is used for definitions.

II. SYSTEM MODEL

Consider a cooperative DF communication system with a source, S , a destination, D , and a MIMO relay of K nodes, R_1, R_2, \dots, R_K , as shown in Fig. 1. The K relays are subject to CFOs and TDs due to the presence of different

local oscillators. We denote the CFOs of the K relays by $(\bar{\nu}_1, \bar{\nu}_2, \dots, \bar{\nu}_K) \subset [0, \nu_{\max}]^K$ and their respective TDs by $(\bar{\tau}_1, \bar{\tau}_2, \dots, \bar{\tau}_K) \subset [0, \tau_{\max}]^K$. The parameters, ν_{\max} and τ_{\max} , can be set as large as desired within the vicinity of practical CFO and TD values. The true unknown parameters will also

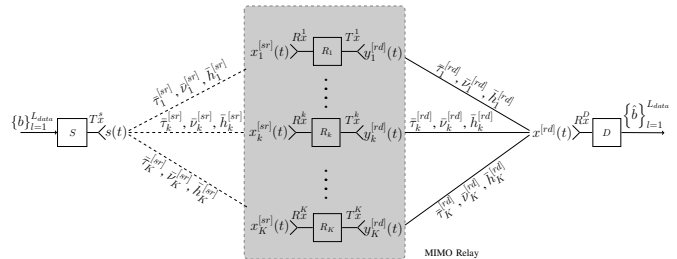


Fig. 1. System model for the distributed MIMO-relay beamforming scheme illustrated during the DT (data transmission) cycles.

carry the superscripts $(\cdot)^{[sr]}$ and $(\cdot)^{[rd]}$ to indicate the communication link to which they belong, i.e., S to R_k and R_k to D , respectively. Most importantly, in stark contrast to previous works on multi-node synchronization which have only dealt so far with TCCs, all the nodes and/or the destination are assumed in this work to be in motion. Hence the second-hop's communication link between each relay node R_k and the destination has a TVC characterized by the Doppler spread σ_{D_k} .

At first, during a synchronization period, the final destination starts by broadcasting a common training sequence, $\mathbf{a}^{[dr]} \triangleq [a^{[dr]}(1), a^{[dr]}(2), \dots, a^{[dr]}(L)]^T$, to all the relays. Hence, every relay node will be able to estimate its own synchronization parameters locally and independently of all others. This approach, in contrast to [3], alleviates the hurdles of estimating closely-spaced TDs and/or CFOs when implemented jointly at the destination. During this pilot transmission (PT) period, the destination broadcasts the following known signal to all the relays:

$$s^{[dr]}(t) = \sum_{l=0}^{L-1} \mathbf{a}^{[dr]}[l+1]g(t-lT), \quad (1)$$

where $g(t)$ is the pulse-shaping function and T is the symbol duration. The continuous-time received signal at the k^{th} relay is given by:

$$x_k^{[dr]}(t) = h_k^{[dr]}(t)s^{[dr]}(t - \bar{\tau}_k^{[dr]})e^{j2\pi\bar{\nu}_k^{[dr]}t} + n_k^{[dr]}(t), \quad (2)$$

where $h_k^{[dr]}(t)$ is a flat-fading Rayleigh channel and $n_k^{[dr]}(t)$ is the additive Gaussian noise component assumed to be temporally white. Using its received signal in (2), each relay will find the estimates, $\hat{\tau}_k^{[dr]}$ and $\hat{\nu}_k^{[dr]}$, for its channel TD and CFO, $\bar{\tau}_k^{[dr]}$ and $\bar{\nu}_k^{[dr]}$, respectively. The signal in (2) is oversampled by a factor $Q = T/T_s$ where T_s is the sampling period. The observation sequence corresponding to

the sampling time instants, $\{nT_s\}_{n=0}^{QL-1}$, is given by:

$$x_k^{[dr]}(n) = h_k^{[dr]}(n) \sum_{l=0}^{L-1} \mathbf{a}^{[dr]}[l+1] g(nT_s - lT - \bar{\tau}_k^{[dr]}) e^{j2\pi \bar{\nu}_k^{[dr]} \frac{n}{Q}} + n_k^{[dr]}(n), \quad (3)$$

where the additive white Gaussian noise is denoted by $n_k^{[dr]}(n) \sim \mathcal{CN}(0, \sigma_{n_k}^2)$. Notice in (3) that we keep using the same notation, $\bar{\nu}_k^{[dr]}$, as in (2) for the normalized (by T_s) CFO between R_k and D , that is for the sake of simplicity.

In order to rewrite (3) in a matrix/vector form, we denote by $\mathbf{x}_k^{[dr]} \triangleq [x_k^{[dr]}(0), x_k^{[dr]}(1), \dots, x_k^{[dr]}(QL-1)]^T$, $\mathbf{h}_k^{[dr]} \triangleq [h_k^{[dr]}(0), h_k^{[dr]}(1), \dots, h_k^{[dr]}(QL-1)]^T$, and $\mathbf{n}_k^{[dr]} \triangleq [n_k^{[dr]}(0), n_k^{[dr]}(1), \dots, n_k^{[dr]}(QL-1)]^T$ the vectors that contain, respectively, the received samples, the channel coefficients, and the noise components. We also introduce the following matrix that is parametrized by the generic TD variable τ :

$$\mathbf{G}(\tau) \triangleq \begin{pmatrix} g(0-T-\tau) & \dots & g(0-LT-\tau) \\ g(T_s-T-\tau) & \dots & g(T_s-LT-\tau) \\ \vdots & \vdots & \vdots \\ g((QL-1)T_s-T-\tau) & \dots & g((QL-1)T_s-LT-\tau) \end{pmatrix}.$$

Starting from (3) and resorting to some straightforward algebraic manipulations, it can be shown for $k = 1, 2, \dots, K$ that we have:

$$\mathbf{x}_k^{[dr]} = \mathbf{\Lambda}(\bar{\nu}_k^{[dr]}) \mathbf{\Omega}(\bar{\tau}_k^{[dr]}) \mathbf{h}_k^{[dr]} + \mathbf{n}_k^{[dr]}, \quad (4)$$

where:

$$\mathbf{\Omega}(\tau) \triangleq \text{diag}\{\mathbf{G}(\tau) \mathbf{a}^{[dr]}\}, \quad (5)$$

$$\mathbf{\Lambda}(\nu) \triangleq \begin{pmatrix} 1 & 0 & \dots & 0 \\ 0 & e^{j2\pi\nu} & 0 & \dots & 0 \\ \vdots & \vdots & \vdots & \vdots & \vdots \\ 0 & \dots & \dots & \dots & e^{j2\pi\nu(QL-1)/Q} \end{pmatrix}. \quad (6)$$

For the sake of clarity, we will only focus on the second hop and assume the first hop's estimation and transmission tasks to be ideal. Indeed, the proposed synchronization algorithm can also be applied at each relay node to obtain the matched filtered samples required to decode the data locally during the data transmission (DT) period. As such, we will drop in (4) and in all the equations of the next section the $[dr]$ superscript thereby leading to:

$$\mathbf{x}_k = \mathbf{\Lambda}(\bar{\nu}_k) \mathbf{\Omega}(\bar{\tau}_k) \mathbf{h}_k + \mathbf{n}_k. \quad (7)$$

III. JOINT TD AND CFO SYNCHRONIZATION

A. Joint TD and CFO ML Estimator

In this section, we start by deriving the log-likelihood function (LLF) that depends on all the unknown parameters observed separately at each relay, i.e., $\nu_k, \tau_k, h_k, \sigma_{n_k}^2$. Since the noise components are assumed to be temporally white and Gaussian distributed, i.e., $\mathbf{n}_k \sim \mathcal{N}(\mathbf{0}, \sigma_{n_k}^2 \mathbf{I}_{QL})$, each vector

\mathbf{x}_k in (7) is also Gaussian distributed. Hence, it can be shown that the *actual* LLF at each relay R_k is given by¹:

$$\mathcal{L}(\nu_k, \tau_k, h_k, \sigma_{n_k}^2) = -\ln(\det\{\mathbf{R}_{\mathbf{x}_k \mathbf{x}_k}\}) - \mathbf{x}_k^H \mathbf{R}_{\mathbf{x}_k \mathbf{x}_k}^{-1} \mathbf{x}_k, \quad (8)$$

where $\mathbf{R}_{\mathbf{x}_k \mathbf{x}_k} = \mathbb{E}\{\mathbf{x}_k \mathbf{x}_k^H\}$ is the covariance matrix of the zero-mean observation vector \mathbf{x}_k whose expression follows from (7) as:

$$\mathbf{R}_{\mathbf{x}_k \mathbf{x}_k} = \mathbf{\Lambda}(\nu_k) \mathbf{\Omega}(\tau_k) \mathbf{R}_{\mathbf{h}_k \mathbf{h}_k} \mathbf{\Omega}(\tau_k)^H \mathbf{\Lambda}(\nu_k)^H + \sigma^2 \mathbf{I}_{QL}, \quad (9)$$

where $\mathbf{R}_{\mathbf{h}_k \mathbf{h}_k} = \mathbb{E}\{\mathbf{h}_k \mathbf{h}_k^H\}$. It is obvious that maximizing $\mathcal{L}(\nu_k, \tau_k, h_k, \sigma_{n_k}^2)$ requires the inversion of a large-size ($QL \times QL$) covariance matrix and the computation of its determinant. In the following, we develop a new solution that avoids these costly calculations. Actually, the new solution relies on a second-order Taylor series approximation of the covariance matrix of the channel, as described in [18], which leads to:

$$\mathbf{R}_{\mathbf{h}_k \mathbf{h}_k} = \frac{\sigma_{h_k}^2}{2} \mathbf{W} \mathbf{W}^H, \quad (10)$$

where \mathbf{W} is defined as follows:

$$\mathbf{W} = [\mathbf{w} \ \mathbf{w}^*], \quad (11)$$

and the two vectors in (11) are given by:

$$\mathbf{w} = \begin{bmatrix} 1 & e^{-j\sigma_{D_k} T_s} & \dots & e^{-j(QL-1)\sigma_{D_k} T_s} \end{bmatrix}^T.$$

Injecting (10) in (9) leads to the following overall covariance matrix approximation:

$$\mathbf{R}_{\mathbf{x}_k \mathbf{x}_k} = \frac{\sigma_{h_k}^2}{2} \mathbf{\Lambda}(\nu_k) \mathbf{C}(\tau_k) \mathbf{C}^H(\tau_k) \mathbf{\Lambda}(\nu_k)^H + \sigma^2 \mathbf{I}_{QL},$$

in which the matrix $\mathbf{C}(\tau_k)$ is defined as follows:

$$\mathbf{C}(\tau_k) \triangleq [\mathbf{c}_1(\tau_k) \ \mathbf{c}_2(\tau_k)] = \mathbf{\Omega}(\tau_k) \mathbf{W}. \quad (12)$$

To find the inverse of $\mathbf{R}_{\mathbf{x}_k \mathbf{x}_k}$ and its determinant, we start by finding the analytical expressions for the eigenvalues of $\mathbf{C}(\tau_k) \mathbf{C}^H(\tau_k)$ and their corresponding eigenvectors. Clearly, the matrix $\mathbf{C}(\tau_k) \mathbf{C}^H(\tau_k)$ is of rank two and has the same non-zero eigenvalues as $\mathbf{C}^H(\tau_k) \mathbf{C}(\tau_k)$. Since the latter is a 2×2 matrix, its eigenvalues can be computed analytically. Indeed, it can be shown that:

$$\mathbf{C}^H(\tau_k) \mathbf{C}(\tau_k) = \begin{pmatrix} \alpha(\tau_k) & \varphi(\tau_k) \\ \varphi(\tau_k)^* & \alpha(\tau_k) \end{pmatrix}, \quad (13)$$

where:

$$\alpha(\tau_k) = \sum_{n=0}^{QL-1} (\Omega_{n,n}(\tau_k))^2, \quad (14)$$

$$\varphi(\tau_k) = \sum_{n=0}^{QL-1} (\Omega_{n,n}(\tau_k))^2 e^{2\sigma_{D_k}(n-1)T_s}. \quad (15)$$

From the roots of the characteristic polynomial of the matrix $\mathbf{C}^H(\tau_k) \mathbf{C}(\tau_k)$ in (13), the two eigenvalues are obtained as follows:

$$\lambda_1 = \alpha(\tau_k) + |\varphi(\tau_k)| \quad \text{and} \quad \lambda_2 = \alpha(\tau_k) - |\varphi(\tau_k)|. \quad (16)$$

¹After dropping the constant terms.

Hence the corresponding unit-norm eigenvectors are given by:

$$\mathbf{v}_1 = \frac{1}{\sqrt{2}} \begin{bmatrix} 1 \\ \frac{\varphi(\tau_k)^*}{|\varphi(\tau_k)|} \end{bmatrix}^T \quad \text{and} \quad \mathbf{v}_2 = \frac{1}{\sqrt{2}} \begin{bmatrix} 1 \\ -\frac{\varphi(\tau_k)^*}{|\varphi(\tau_k)|} \end{bmatrix}^T.$$

Since λ_1 and λ_2 are also the two non-zero eigen-values of $\mathbf{C}(\tau_k)\mathbf{C}(\tau_k)^H$, the singular value decomposition (SVD) of the matrix $\mathbf{C}(\tau_k)$ is obtained as follows:

$$\mathbf{C}(\tau_k) = \mathbf{U}(\tau_k)\mathbf{\Sigma}(\tau_k)^{1/2}\mathbf{V}(\tau_k)^H, \quad (17)$$

where:

$$\mathbf{\Sigma}(\tau_k) \triangleq \text{diag}\{\lambda_1, \lambda_2\} \quad \text{and} \quad \mathbf{V}(\tau_k) \triangleq [\mathbf{v}_1 \quad \mathbf{v}_2]. \quad (18)$$

Moreover, since $\mathbf{V}(\tau_k)^H\mathbf{V}(\tau_k) = \mathbf{I}_2$, then $\mathbf{U}(\tau_k) = [\mathbf{u}_1 \quad \mathbf{u}_2]$ can be expressed as follows:

$$\mathbf{U}(\tau_k) = \mathbf{C}(\tau_k)\mathbf{V}(\tau_k)^H\mathbf{\Sigma}(\tau_k)^{1/2}. \quad (19)$$

Therefore, it follows that:

$$\mathbf{u}_1 = \frac{1}{\sqrt{2\lambda_1}} \left(\mathbf{c}_1(\tau_k) + \frac{\varphi(\tau_k)^*}{|\varphi(\tau_k)|} \right), \quad (20)$$

$$\mathbf{u}_2 = \frac{1}{\sqrt{2\lambda_2}} \left(\mathbf{c}_2(\tau_k) - \frac{\varphi(\tau_k)^*}{|\varphi(\tau_k)|} \right). \quad (21)$$

Now, by injecting (17) back into (12), it follows that:

$$\mathbf{R}_{\mathbf{x}_k\mathbf{x}_k} = \sigma_{n_k}^2 \left(\frac{\rho}{2} \mathbf{B}(\nu_k, \tau_k) \mathbf{\Sigma}(\tau_k) \mathbf{B}(\nu_k, \tau_k)^H + \mathbf{I}_{QL} \right), \quad (22)$$

where $\mathbf{B}(\nu_k, \tau_k) = \mathbf{\Lambda}(\nu_k) \mathbf{U}(\tau_k)$ and $\rho_k = \sigma_{h_k}^2 / \sigma_{n_k}^2$ is the signal-to-noise ratio (SNR). Using the Woodbury identity [19], the inverse of (22) can be computed analytically as follows:

$$\mathbf{R}_{\mathbf{x}_k\mathbf{x}_k}^{-1} = \frac{1}{\sigma_{n_k}^2} \mathbf{I}_{QL} - \frac{1}{\sigma_{n_k}^2} \mathbf{B} \left(\frac{2}{\rho_k} \mathbf{\Sigma}^{-1} + \mathbf{B}^H \mathbf{B} \right)^{-1} \mathbf{B}^H, \quad (23)$$

from which, the matrix and vector arguments have been removed for the sake of simplicity. Next, exploiting the fact that \mathbf{u}_1 and \mathbf{u}_2 are orthogonal with unit norms, the inverse of the covariance matrix in (23) can be written as follows:

$$\mathbf{R}_{\mathbf{x}_k\mathbf{x}_k}^{-1} = \frac{1}{\sigma_{n_k}^2} \mathbf{I}_{QL} - \frac{1}{\sigma_{n_k}^2} \mathbf{B}(\nu_k, \tau_k) \mathbf{\Gamma}(\tau_k) \mathbf{B}(\nu_k, \tau_k)^H, \quad (24)$$

where:

$$\mathbf{\Gamma}(\tau_k) = \text{diag} \left\{ \frac{\rho\lambda_1}{2 + \rho\lambda_1}, \frac{\rho\lambda_2}{2 + \rho\lambda_2} \right\}. \quad (25)$$

Moreover, from (22), it can be shown that the determinant of $\mathbf{R}_{\mathbf{x}_k\mathbf{x}_k}$ is given by:

$$\det\{\mathbf{R}_{\mathbf{x}_k\mathbf{x}_k}\} = \frac{(\sigma_{n_k}^2)^{QL}}{4} (\rho\lambda_1 + 2)(\rho\lambda_2 + 2). \quad (26)$$

Finally, by injecting (24) and (26) back into (8), the LLF reduces to:

$$\begin{aligned} \mathcal{L}(\nu, \tau, \sigma_n^2) &= -\ln((\rho\lambda_1 + 2)(\rho\lambda_2 + 2)) \\ &\quad + \frac{1}{\sigma_n^2} \left\| \mathbf{\Gamma}(\tau_k)^{1/2} \mathbf{B}(\nu_k, \tau_k)^H \mathbf{x}_k \right\|^2. \end{aligned} \quad (27)$$

By expanding the norm in (27), the LLF can be expressed as follows:

$$\begin{aligned} \mathcal{L}(\nu, \tau, \sigma_n^2) &= -\ln((\rho\lambda_1 + 2)(\rho\lambda_2 + 2)) \\ &\quad + \frac{1}{\sigma_n^2} \sum_{i=1}^2 \frac{\rho\lambda_i}{2 + \rho\lambda_i} \left| \mathbf{u}_i^H \mathbf{\Lambda}(\nu)^H \mathbf{x}_k \right|^2, \end{aligned} \quad (28)$$

and the joint ML estimates of ν_k and τ_k , assuming perfect knowledge of the Doppler spread σ_{D_k} , are obtained as the solution to the following two-dimensional optimization problem:

$$[\hat{\nu}_k, \hat{\tau}_k] = \underset{\nu, \tau}{\text{argmax}} \mathcal{L}(\nu, \tau). \quad (29)$$

Note here that the estimates of the SNR and the noise variance are obtained using the same approach adopted in [20]. Moreover, by closely inspecting the expression in (28), we observe that the underlying LLF can be evaluated more efficiently at each TD candidate value, and all CFO candidate values using the fast Fourier transform (FFT).

B. Cramer Rao Lower Bound (CRLB)

In the TVC case, the CLRB was previously derived in [21] for the Doppler spread estimation. In the following, we extend it to joint CFO and TD estimation for performance benchmarking. Recall that the covariance matrix of the received signal is given by:

$$\begin{aligned} \mathbf{R}_{\mathbf{x}_k\mathbf{x}_k} &= \mathbf{\Lambda}(\bar{\nu}_k) \mathbf{\Omega}(\bar{\tau}_k) \mathbf{E}\{\mathbf{h}_k \mathbf{h}_k^H\} \mathbf{\Omega}(\bar{\tau}_k)^H \mathbf{\Lambda}(\bar{\nu}_k)^H + \bar{\sigma}_{n_k}^2 \mathbf{I}_{QL} \end{aligned} \quad (30)$$

Let $\zeta = [\bar{\tau}_k, \bar{\nu}_k, \bar{\sigma}_{n_k}^2]^T$ be a vector that contains all the parameters of interest, then the $(k, l)^{th}$ element of the Fisher information matrix (FIM) can be written as follows:

$$[\mathbf{J}(\zeta)]_{k,l} = \text{trace} \left[\mathbf{R}_{\mathbf{x}_k\mathbf{x}_k}^{-1} \frac{\partial \mathbf{R}_{\mathbf{x}_k\mathbf{x}_k}}{\partial \zeta_k} \mathbf{R}_{\mathbf{x}_k\mathbf{x}_k}^{-1} \frac{\partial \mathbf{R}_{\mathbf{x}_k\mathbf{x}_k}}{\partial \zeta_l} \right]. \quad (31)$$

The CRLBs for the TD and CFO parameters are obtained by finding the inverse of the FIM in (31) and then taking its first and second diagonal entries, respectively.

IV. DISTRIBUTED TRANSMIT BEAMFORMING AT THE MIMO RELAY

The ML estimator is run at each relay node with the transceiver illustrated in Fig. 2. During a PT period, each node performs a channel parameter estimation task. During the DT period, each relay will transmit the useful data to the destination while ensuring that the signal is modified properly using the TD, CFO and channel estimates made available during the PT period. Note that the synchronization parameters are expected to vary with time, but actually at a rate much slower than the channel time-variations. Therefore the synchronization parameters will be refreshed once each P consecutive DT periods. Right after the synchronization period, the destination will periodically transmit to all the relays, at each p^{th} period, a training sequence \mathbf{a}_p that only contains L_{ch} pilot symbols, i.e., $\mathbf{a}^{[dr]} = \{a_l^{[dr]}\}_{l=1}^{L_{\text{ch}}}$. The

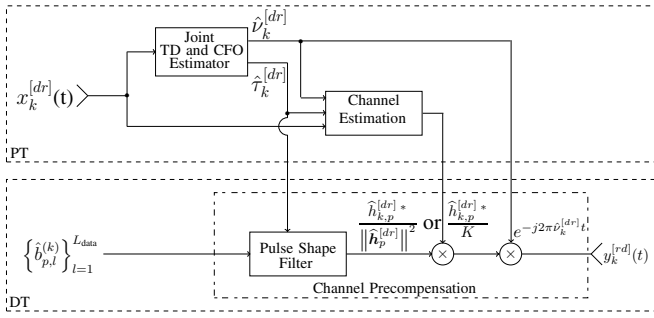


Fig. 2. Block diagram of the DF transceiver at the k^{th} relay.

latter will be exploited by each relay to update its channel state information (CSI) with respect to the destination. More specifically, the corresponding oversampled signal denoted² here as $\tilde{\mathbf{x}}_k^{[dr]}$ is processed by relay R_k to find the ML estimate of its own complex-valued channel coefficient of the D -to- R_k link during the $\{p^{th}\}_{p=1}^P$ period, as follows :

$$\hat{h}_{k,p}^{[dr]} = \frac{1}{\|\mathbf{r}(\hat{\nu}_k, \hat{\tau}_k)\|^2} \mathbf{r}^H(\hat{\nu}_k, \hat{\tau}_k) \tilde{\mathbf{x}}_k^{[dr]}, \quad k = 1, 2, \dots, K, \quad (32)$$

where:

$$\mathbf{r}(\nu, \tau) = \mathbf{\Lambda}(\nu) \mathbf{G}(\tau) \mathbf{a}^{[dr]}. \quad (33)$$

To ensure that the signals from all the relays arrive at the receiver coherently and thus combine constructively, the relays must adjust their carrier frequencies, carrier phases, and symbol timings as follows:

- The signal carrying the useful data to be transmitted by the k^{th} relay is delayed as follows:

$$s(t - \hat{\tau}_k^{(\text{comp})}) = \sum_{l=0}^{L_{\text{data}}-1} b_{p,l+1} g(t - lT - \hat{\tau}_k^{(\text{comp})}), \quad (34)$$

where $\{b_{p,l}\}_{l=1}^{L_{\text{data}}}$ are the symbols containing the useful data during the p^{th} period assuming here perfect transmission links between the source and the relays, and $\hat{\tau}_k^{(\text{comp})} = \tau_{\text{max}} - \hat{\tau}_k^{[dr]}$.

- The relay node pre-compensates its CFO by de-rotating the signal in (34) as follows:

$$e^{-j2\pi\hat{\nu}_k^{[dr]}t} s(t - \hat{\tau}_k^{(\text{comp})}). \quad (35)$$

- By relying on the channel reciprocity property of time-division duplex (TDD) schemes, we pre-compensate the channel phase and match its amplitude with the complex channel estimate to generate the following transmit signal $y_k(t)$ at each relay:

$$y_k(t) = \frac{\hat{h}_{k,p}^{[dr]*}}{\|\hat{\mathbf{h}}_p^{[dr]}\|^2} e^{-j2\pi\hat{\nu}_k t} s(t - \hat{\tau}_k^{(\text{comp})}), \quad (36)$$

where $\hat{h}_{k,p}^{[dr]}$ is the channel estimate at the k^{th} relay obtained from (32) and $\hat{\mathbf{h}}_p^{[dr]} = [\hat{h}_{1,p}^{[dr]}, \hat{h}_{2,p}^{[dr]}, \dots, \hat{h}_{K,p}^{[dr]}]^T$.

²Note here that $\tilde{\mathbf{x}}_k^{[dr]}$ is equivalent to $\mathbf{x}_k^{[dr]}$ in (7) using, however, another training sequence transmitted specifically for channel estimation purposes.

In (36), we need to have the channel estimates over all $D - R$ links available at each relay node for the sole purpose of calculating the square norm of the K -dimensional $D - R$ vector channel. The latter can be fed back by the destination. Alternatively, to avoid any additional overhead, it can be simply approximated by its average value K as follows:

$$y_k(t) \approx \frac{\hat{h}_{k,p}^{[dr]*}}{K} e^{-j2\pi\hat{\nu}_k t} s(t - \hat{\tau}_k^{(\text{comp})}). \quad (37)$$

At the destination, the received signal, $x_p^{[rd]}(t)$, which is the superposition of all the pre-synchronized signals transmitted by the K relays, can be expressed as follows:

$$x_p^{[rd]}(t) = \sum_{k=1}^K h_{k,p}^{[rd]}(t) e^{-j2\pi\nu_k t} y_k(t - \tau_k) + w(t), \quad (38)$$

where $h_{k,p}^{[rd]}(t)$ is the true time-varying channel pertaining to the k^{th} relay. By substituting $y_k(t)$ in (38) with its expression in (36), the received signal is rewritten as follows:

$$x_p^{[rd]}(t) = \sum_{k=1}^K h_{k,p}^{[rd]}(t) \frac{\hat{h}_{k,p}^{[dr]*}}{\|\hat{\mathbf{h}}_p^{[dr]}\|^2} e^{j2\pi(\hat{\nu}_k^{[dr]} - \nu_k^{[dr]})t} s(t - \hat{\tau}_k^{(\text{comp})} - \tau_k^{[dr]}) + w(t). \quad (39)$$

V. SIMULATION RESULTS

In the following, we discuss our simulation results at both the component and link levels when all previous works would stop short from moving to the more time consuming yet much more insightful link level. In all our simulations, we assume as would be expected in practice that the K relays are co-located at about the same distance and moving at the same relative speed from the destination whether the latter is stationary or also in motion itself. Under this assumption, the average SNR and the Doppler frequency are assumed to be the same over all R-D and D-R links. Nevertheless, both the SNR and Doppler frequency values could be different from one second-hop link to another. In the following, we will investigate in different scenarios the estimation accuracy of the tested synchronization parameter estimators in terms of the normalized mean square error (NMSE) before assessing their link-level performance.

A. Component-Level Simulations

In all component-level simulations, we consider a training sequence, $\mathbf{a}^{[dr]}$, of $L_{\text{sync}} = 32$ QPSK symbols and a square root raised-cosine shaping-pulse filter (SRRC) with a roll-off factor $\rho = 0.3$. In Fig. 3, we compare the proposed technique against the SAGE algorithm in [3], the sole benchmark available in the literature dealing with multi-node TD and CFO synchronization, and the CRLBs derived in Section III.B in terms of NMSE performance. We see that all the mentioned techniques approach the CRLB under the TCC assumption nearly achieved at $F_D = 0.1$ Hz. Indeed, since the SAGE technique is built upon such approximation, it provides accurate estimates with a small degradation at high SNRs.

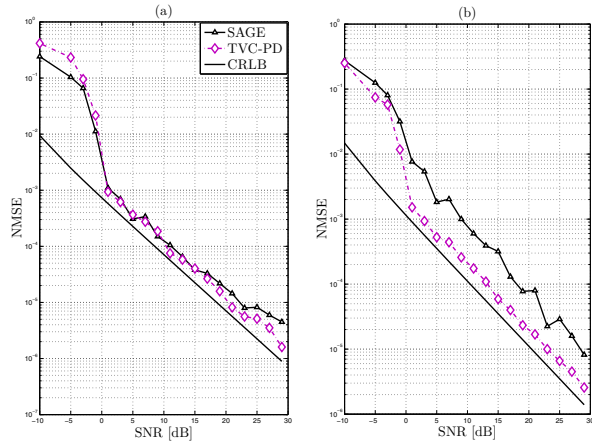


Fig. 3. CRLB and NMSE vs SNR of the ML TVC, ML TCC, and SAGE techniques vs the SNR with $F_{D_k} = 0.1$ Hz and *uniform Jakes'* model for: (a) the TDs and (b) the CFOs.

This degradation is caused by the error floor resulting from this approximation made to avoid grid search maximization.

In Fig. 4, we tackle a more challenging case with sig-

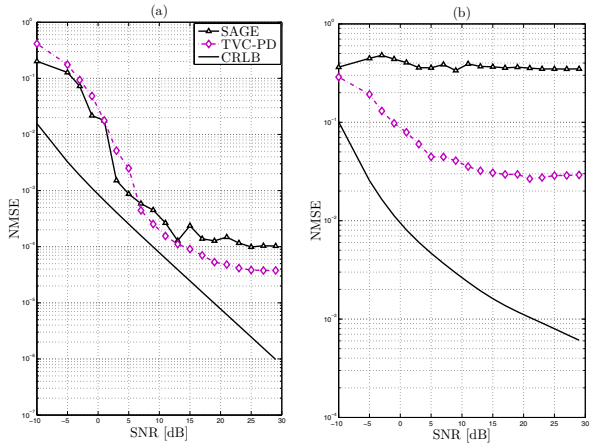


Fig. 4. CRLB and NMSE vs SNR of the ML TVC, ML TCC, and SAGE techniques vs the SNR with $F_{D_k} = 500$ Hz and *uniform Jakes'* model for: (a) the TDs and (b) the CFOs.

nificantly higher Doppler value $F_D = 500$ Hz. We observe that the new technique outperforms the TCC-based technique (i.e., SAGE) in terms of CFO and TD estimation accuracy, especially at medium and high SNR values. Clearly, the TCC assumption does not hold for high Dopplers. As such, the SAGE algorithm fails to converge to the global maximum and exhibits poor performance. Moreover, the perfect knowledge of the Doppler spread allows the ML TVC-PD technique to provide better estimates.

To better investigate the effect of Doppler frequency on the synchronization accuracy, we plot in Fig. 5 the NMSE of all techniques against the Doppler. Obviously ML TVC-PD outperform the TCC-based technique (i.e., SAGE) over a wide Doppler range (i.e., $F_{D_k} \leq 100$ Hz). As the Doppler increases, the TCC-based technique start experiencing serious difficulties to converge to the global maximum that translate into extremely poor TD and CFO estimation accuracies.

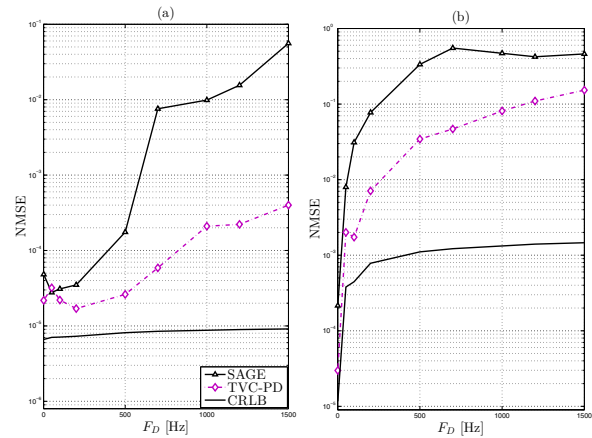


Fig. 5. CRLB and NMSE vs F_D of the ML TVC and SAGE techniques with $SNR = 20$ dB and *uniform Jakes'* model for: (a) the TDs, and (b) the CFOs.

B. Link-Level Simulations

Our link-level simulations were run using the key setup parameters listed in Table I.

TABLE I
SIMULATION PARAMETERS

Parameters	Symbol	Values
Symbol period	T	1/14 ms
Number of relays	K	2
Maximum Doppler shift	$\{F_{D_k}\}_{k=1}^K$	{0.1, 500} Hz
Oversampling factor	Q	2
Roll-off factor	ρ	0.3
TDs	τ_k	Uniformly random (i.i.d.)
CFOs	ν_k	Uniformly random (i.i.d.)
$R_k - D$ channel	\mathbf{h}_k	Rayleigh random (i.i.d.)

Fig. 6 depicts the resulting throughput for three different modulation orders (QPSK, 16-QAM and 64-QAM) and K relays. We consider in Figs. 6 (a) and 6 (b) the case where all K relay-destination links have the same maximum Doppler frequency shift of 15 and 100 Hz, respectively. For a given modulation order M , the throughput is obtained from the symbol error rate (SER) as follows:

$$\text{Throughput} = \frac{1}{T} \log_2(M)(1 - \text{SER})(1 - R), \quad (40)$$

where R is the overhead ratio. Note here that the latter is computed over a period that spans L_{sync} symbols for synchronization and P periods each of which includes $L_{\text{ch}} = 2$ pilot symbols followed by $L_{\text{data}} = 12$ information-bearing symbols. As such, the overhead ratio is given by:

$$R = \frac{L_{\text{sync}} + L_{\text{ch}}P}{L_{\text{sync}} + (L_{\text{ch}} + L_{\text{data}})P}. \quad (41)$$

Our simulations were obtained for $L_{\text{sync}} = 32$ and $P = 3$. Note here that the overhead ratio associated with the synchronization period becomes negligible for such large value of P . The latter cannot, however, be increased indefinitely as it is dictated by the required refreshment rate P that better copes with the time variations of the synchronization parameters.

We see from Fig. 6 (a) that QPSK transmissions, among the different considered modulations, provide higher throughput for SNR values below 9 dB. When the SNR ranges between 10

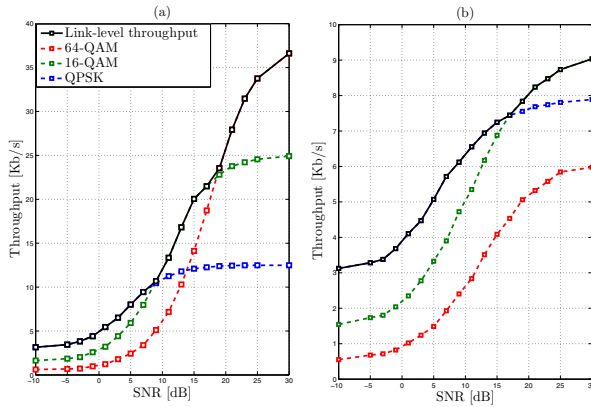


Fig. 6. Link-level throughput vs SNR for ML TVC-PD at $K = 2$ relays and a refreshment rate $P = 100$ for: (a) $\{F_{D_k}\}_{k=1}^K = 0.1$ Hz, and (b) $\{F_{D_k}\}_{k=1}^K = 500$ Hz.

dB and 19 dB, 16-QAM becomes more suitable whereas 64-QAM dominates when the SNR exceeds 20 dB. The resulting throughput curve assuming an adaptive (i.e., SNR-dependent) modulation is depicted by the black curve.

In Fig. 6 (b), we show the performance of the proposed distributed beamforming scheme at a higher Doppler $F_{D_k} = 500$ Hz (i.e., fast TVCs). We see that QPSK transmissions become more appropriate over a large range of SNR (i.e., SNR = 17 dB). Indeed, at low Doppler values, the phase estimates of (32) provide accurate values since the channel varies slowly during the same period. Hence, the decoder at the destination is able to accurately estimate the transmitted symbols. In the case of high mobility, the channel varies rapidly during the same period, leading to a more severe degradation of the channel estimates. Such results affect the decoding process especially with high modulation which are more sensitive to phase shifts.

VI. CONCLUSION

In this paper, we addressed the problem of time and frequency synchronization in cooperative systems over time-varying channels. For the proposed technique, we assume perfect knowledge of the Doppler spread to provide accurate TD and CFO synchronization estimates. We showed under the TCC assumption that all techniques exhibit approximately the same performance. However, when the Doppler increases, the TCC-based technique exhibit poor performances while the new ML TVC continues to provide accurate estimates.

REFERENCES

- [1] A. Sendonaris, E. Erkip, and B. Aazhang, "User cooperation diversity. Part I. System description," *IEEE Trans. Commun.*, vol. 51, no. 11, pp. 1927-1938, Nov. 2003.
- [2] Y. Jing and H. Jafarkhani, "Network beamforming using relays with perfect channel information," *IEEE Trans. Inf. Theory*, vol. 55, no. 6, pp. 2499-25178, June 2009.
- [3] A. A. Nasir, H. Mehrpouyan, S. Durani, R. A. Kennedy, and S. D. Blostein, "Timing and carrier synchronization with channel estimation in multi-relay cooperative networks," *IEEE Trans. Signal Process.*, vol. 60, no. 2, pp. 793-811, Feb. 2012.
- [4] H. Wang, X.-G. Xia, and Q. Yin, "Computationally efficient equalization for asynchronous cooperative communications with multiple frequency offsets," *IEEE Trans. Wireless Commun.*, vol. 8, no. 2, pp. 648-655, Feb. 2009.

- [5] Y.-S. Tu and G. Pottie, "Coherent cooperative transmission from multiple adjacent antennas to a distant stationary antenna through AWGN channels," in *Proc. Veh. Technol. Conf. (VTC)*, Birmingham, AL, USA, May 2002.
- [6] X. Li, C. Xing, Y.-C. Wu, and S. C. Chan, "Timing estimation and resynchronization for amplify-and-forward communication systems," *IEEE Trans. Signal Process.*, vol. 58, no. 4, pp. 2218-2229, Apr. 2010.
- [7] H. Mehrpouyan and S. D. Blostein, "Estimation, training, and effect of timing offsets in distributed cooperative networks," in *Proc. IEEE Global Commun. Conf. (GLOBECOM)*, Miami, FL, Dec. 2010.
- [8] M. T. Hossain, D. B. Smith, and S. Kandeepan, "Timing synchronization for cooperative communications with detect and forward relaying," *Springer J. Wireless Pers. Commun.*, 2010.
- [9] X. Li, Y. C. Wu, and E. Serpedin, "Timing synchronization in decode-and-forward cooperative communication systems," *IEEE Trans. Signal Process.*, vol. 57, no. 4, pp. 1444-1455, Apr. 2009.
- [10] H. Mehrpouyan and S. D. Blostein, "Bounds and algorithms for multiple frequency offset estimation in cooperative networks," *IEEE Trans. Wireless Commun.*, vol. 10, no. 4, pp. 1300-1311, Apr. 2011.
- [11] O. Besson and P. Stoica, "On parameter estimation of MIMO flat-fading channels with frequency offsets," *IEEE Trans. Signal Process.*, vol. 51, no. 3, pp. 602-613, Mar. 2003.
- [12] T. Pham, A. Nallanathan, and Y. Liang, "Joint channel and frequency offset estimation in distributed MIMO flat-fading channels," *IEEE Trans. Wireless Commun.*, vol. 7, no. 2, pp. 648-656, Feb. 2008.
- [13] Y. Yao and T. Ng, "Correlation-based frequency offset estimation in MIMO system," in *Proc. IEEE Veh. Technol. Conf. (VTC)*, Orlando, FL, Oct. 2003.
- [14] J.-H. Lee and S.-C. Kim, "Time and frequency synchronization for OFDMA uplink system using the SAGE algorithm," *IEEE Trans. Wireless Commun.*, vol. 6, no. 4, pp. 1176-1181, Apr. 2007.
- [15] M. Morelli, "Time and frequency synchronization for the uplink of an OFDMA system," *IEEE Trans. Commun.*, vol. 52, no. 2, pp. 296-396, Feb. 2004.
- [16] M.A Alvarez and U. Spagnolini, "Distributed time and carrier frequency synchronization for dense wireless networks," *IEEE Trans. Signal Inform. Process. Over Netw.*, pp. 1-13, Mar. 2018.
- [17] R. He, G. Wang, Z. Zhong, A. F. Molisch, C. Briso-Rodriguez and C. Oestges, "High-speed railway communications: From GSM-R to LTE-R," *IEEE Trans. Veh. Technol. Mag.*, vol. 11, no. 3, pp. 49-58, Mar. 2016.
- [18] F. Bellili, Y. Selmi, S. Affes, and A. Ghayeb, "A low-cost and robust maximum likelihood joint estimator for the Doppler spread and CFO parameters over flat-fading Rayleigh channels," *IEEE Trans. Commun.*, vol. 65, no. 8, pp. 3467-3478, Aug. 2017.
- [19] K. B. Petersen and M. S. Pedersen, *The Matrix Cookbook*, Technical University of Denmark, Nov. 2012, Version 20121115. [Online]. Available: <http://www2.imm.dtu.dk/pubdb/p.php?3274>.
- [20] M. Souden, S. Affes, J. Benesty, and R. Bahroun, "Robust Doppler spread estimation in the presence of a residual carrier frequency offset," *IEEE Trans. Signal Process.*, vol. 57, no. 10, pp. 4148-4153, Oct. 2009.
- [21] C. Tepedelenlioglu, "Performance analysis of velocity (Doppler) estimators in mobile communications," *Proc. IEEE Int. Conf. Acoustic, Speech Signal Process. (ICASSP)*, Orlando, USA, May 2002.